

Mechanisms of Defect Generation and Clustering in CH₃S Self-Assembled Monolayers on Au(111)

P. Carro,[†] D. Torres,^{‡,⊥} R. Diaz,[§] R. C. Salvarezza,^{||} and F. Illas^{*,‡}

[†]Departamento de Química Física, Instituto de Materiales y Nanotecnología, Universidad de La Laguna, Tenerife, Spain

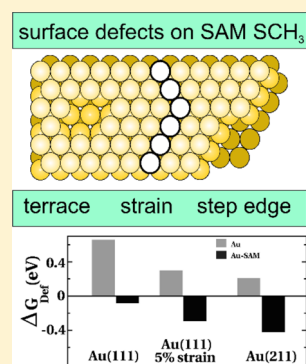
[‡]Departament de Química Física & Institut de Química Teòrica i Computacional (IQTCUB), Universitat de Barcelona, C/Martí i Franquès 1, 08028 Barcelona, Spain

[§]Unidad de Procesos Electroquímicos, Instituto IMDEA Energía, Avda. Ramón de la Sagra, 3, Móstoles (Madrid), Spain

^{||}Universidad Nacional de La Plata - CONICET, Sucursal 4 Casilla de Correo 16 (1900) La Plata, Argentina

ABSTRACT: Periodic density functional calculations probe that step edges play a key role as source of defects during self-assembly. It is shown that the self-assembly process strongly reduces the energy required to strip an atom from the gold surface, locally increasing the concentration of surface defects. The thermodynamic driving force for the atom stripping is considerably more favorable along step-edge lines within the self-assembly than on the higher-coordinated terrace sites. Furthermore, the clustering of surface defects is considered, and we probe that the formation of aggregates of vacancies in the form of vacancy pits significantly stabilizes the self-assembly on the terraces of gold, where the role of the step edges is expected to be less significant. The high stability of pit-like structures arises from a balance between the corrugation and the enhanced bonding of defect-rich substrates. Our results demonstrate the important role that step edges play during assembly and could be very valuable for discovering defect-free assembled structures.

SECTION: Surfaces, Interfaces, Porous Materials, and Catalysis



Understanding the mechanisms for nucleation and the factors influencing the molecular ordering of self-assembled monolayers (SAMs) of alkanethiolates has long been a goal for surface scientists. The ($\sqrt{3} \times \sqrt{3}$)-R30° lattice formed by methyl thiolate on Au(111) is of particular interest because it provides a rather simple model to understand the basic aspects of the self-assembly of organic molecules.¹⁻⁴ However, even in this widely studied system, fundamental controversies remain, and little is directly known about the headgroup-substrate structure and interaction. SCH₃-Au SAMs are usually produced by exposing Au surfaces to gas-phase dimethyl disulfide (CH₃SSCH₃, DMDS) that spontaneously forms mercaptomethyl radical (SCH₃, MT) due to a cleavage of disulfide bonds.⁵ Only recently, there has been an increasing awareness that surface defects present on the Au substrate may play an important role in the molecular ordering. Recent density functional (DF) calculations confirmed that the interface was characterized by a large atomic roughness with both Au adatoms (Au_{ad}) and vacancies being present.⁶ Also, STM studies identified the extraction of surface Au atoms during self-assembly,⁷ and DF calculations confirmed the presence of Au adatoms at the interface.⁸

It is now accepted that the SAM on the Au surface consists of MT-Au_{ad} or MT-Au_{ad}-MT moieties.¹ The formation of these species requires sources and sinks of defects, and the nature of those sources is still unclear. Many defect structures including step edges, kinks, and faces have been hypothesized to be a feasible source of surface defects.^{1,9} Step edges are well-known

sources of defects, and the role of these structures is well-appreciated in surface science¹⁰ and catalysis.¹¹ Step-edges sites enable enhanced binding of reactants as a result of their reduced coordination.^{11,12} Regions of high strain can also act as source of defects during self-assembly. The clean Au(111) surface is reconstructed, accommodating one extra Au atom on the surface for every 22 bulk lattice constants, which gives rise to a surface densification. However, adsorbed thiols are able to lift the reconstruction expelling the herringbone elbows.¹³ Even the bulk-terminated gold substrate was suggested to be involved on the self-assembly, and a significant portion of the Au surface can be removed during the self-assembly process forming etch pits.¹⁴ The idea dates back to pioneering experimental work of Poirier and Pylant, who revealed the presence of small depressions a few nanometers in size, which are not observed on bare Au.¹⁵ Indeed, etch pits are known to be one of the weakest areas of the self-assembled films in terms of attack and degradation by oxidizing species. Because of the complex nature of the interface, very little knowledge exists concerning the role of vacancy pit formation that accompanies the self-assembly process or the origin of surface defects within the self-assembly, and understanding these aspects calls for further investigation.

Here we present self-consistent periodic DF calculations that address the role of defect structures as a source of surface

Received: June 1, 2012

Accepted: July 26, 2012

defects during MT self-assembly on Au(111). We show that the self-assembly process strongly increases the thermodynamic driving force to strip an atom from the Au surface. The atom stripping is considerably more favored along step-edge lines within the SAM than on the higher-coordinated terrace sites. Because the concentration of surface vacancies correlates with the vacancy formation energy, our results indicate that the self-assembly nucleation process will lead to a local increase in the equilibrium concentration of vacancies, and structures such as step edges, dislocations, or elbows of the Au(111) herringbone reconstruction will act as sources of defects during the assembly. We also analyze the mechanisms of vacancy clustering and show that the formation of vacancy aggregates in the form of pits significantly reduces the Gibbs free energy of the self-assembled structure, thus stabilizing the phase. We suggest that the role of vacancy pits is thus to regulate the concentration of vacancies that are supersaturated as a consequence of the self-assembly process. The high stability of pit-like structures arises from a balance between the corrugation and the enhanced bonding of defect-rich substrates. Our results, demonstrating the close connection existing between self-assembly and defect structures, have important implications on the fabrication of self-assembled structures and could help improve the quality of self-assembled phases.

The DFT calculations employ the projector-augmented wave method¹⁶ to describe the effect of the atomic cores in the valence density in conjunction with a plane-wave basis set (cutoff energy of 400 eV) to expand the valence density and the PW91 implementation of the generalized gradient approach to electronic exchange and correlation energy, which predicts binding energies and geometries in qualitative agreement with experiment.^{17,18} To model the MT adsorption on an unreconstructed Au surface and the formation of defects due to SAM, we employed a $(3\sqrt{3} \times 3\sqrt{3})\text{-R}30^\circ\text{-9CH}_3\text{S}$ surface structure, previously observed for this molecule in the high coverage regime.^{8,19} This unit cell, with an area of 200 \AA^2 , was large enough to describe vacancy-pits with approximate area of 70 \AA^2 or lower. Other superlattices such as the $c(4 \times 2)$ were observed for other molecules, depending on factors such as the chain length and surface defects.²⁰ This lattice, however, has never been observed for MT on Au(111), and hence in this work we will consider only the $(\sqrt{3} \times \sqrt{3})\text{-R}30^\circ$ MT lattice. The slab model consists of five metallic layers with a total of 135 Au atoms in the unit cell interleaved by a vacuum space of $\sim 10 \text{ \AA}$. Different amounts of Au atoms were considered in the first layer to mimic the formation of vacancy pits. The two outermost atomic metal layers as well as the atomic coordinates of MT moieties were allowed to relax without further constraints. Because of the large unit cell size, the Brillouin zone integration was carried out at the Γ point only. We considered an additional Au(211) surfaces model to be representative of stepped surfaces. This has been represented by a 4×3 surface unit cell and single MT species, with a terrace that is four atoms deep and three atoms wide (total of 48 atoms per unit cell). A vacuum of $\sim 10 \text{ \AA}$ separates any two successive slabs, and nine special Monkhorst-Pack k -points²¹ were used for integration in the reciprocal space. Surface relaxation is allowed in the top two Au layers of the slab. All calculations have been carried out using the VASP package.²²

To compare the stability of surface unit cells with different number of atoms, we computed formation Gibbs free surface energies following the ab initio atomic thermodynamics

formalisms.²³ The Au vacancy formation free energy is defined as

$$\Delta G_{\text{Def}} = \frac{G_{\text{Cell}} + N_{\text{Def}}\mu_{\text{Au}} - G_{\text{Cell},0}}{N_{\text{Def}}} \quad (1)$$

determined with respect to bulk Au and computed according to previous studies using total energies from DFT calculations.²⁴ G_{Cell} and $G_{\text{Cell},0}$ are, respectively, the Gibbs free energy of the Au substrate with N_{Def} vacancies and of the relaxed undefective surface, whereas μ_{Au} stands for the standard chemical potential of bulk Au. Entropy contributions to the vacancy formation energy are not included because, in practice, this contribution is small, on the order of $K_{\text{B}}T$, at room temperature (RT, 300 K), where K_{B} is the Boltzmann constant.²⁵ We further defined a generalized formation free energy of a self-assembled phase as

$$\Delta G_{\text{SAM}} = G_{\text{Tot}} - N_{\text{Au}}\mu_{\text{Au}} - N_{\text{MT}}\frac{\mu_{\text{DMDS}}}{2} - G_0 \quad (2)$$

which depends on the Gibbs free energies and chemical potentials of the constituents and can be computed using total energies from DFT calculations. G_{Tot} refers to the Gibbs free energy of the surface model containing the SAM in the presence of Au surface vacancies. N_{Au} and N_{MT} are the number of Au atoms and of MT moieties in the unit cell, respectively. G_0 defined as $G_{\text{Cell},0} - N_{\text{Au},0}\mu_{\text{Au}}$ refers to the Gibbs free energy of formation of the bare Au surface in the absence of self-assembly and surface defects, where $N_{\text{Au},0}$ is the number of Au atoms in the bulk-like cell. We considered the bulk limit of Au chemical potential $\mu_{\text{Au}} = E_{\text{Au}}^{\text{bulk}}$ and the DMDS molecule as gas-phase reference at standard pressure. Entropy change for DMDS adsorption was calculated to be 0.84 eV at 300 K, neglecting the entropy contribution of the surface-adsorbed species. We added the configurational entropy for the vacancy arrangement to the generalized formation free energy according to previous studies.²⁶ The surface defect coverage, Θ_{Def} was defined as the number of Au vacancies per surface atom in the bulk-like cell. For each Θ_{Def} we considered all possible defect-arrangements and selected the one with lowest total Gibbs free energy.

First, we consider the mechanisms of defect-generation in the self-assembled structure by calculating vacancy-formation energies. ΔG_{Def} quantifies the stability of a vacancy in the metal and determines the likelihood of its formation: the more negative this energy, the more favored the adatom ejection (and vacancy formation). The presence of dislocations or Au(111) surface herringbone reconstruction is known to cause localized strain on the surface of gold. The release of Au atoms from the surface upon the formation of the SAM (in particular, from the "elbows" in the herringbone structure) is one of the possible adatom-generation mechanisms. To address the generation of defects on strained gold regions, we considered a Au(111) surface under uniaxial compressive strain by reducing 5% the lattice constant parallel to the surface. We focused our studies on Au(111) slabs with 5% compressive strain because a compression of $\sim 4.5\%$ was observed experimentally along the $\langle 110 \rangle$ direction of the reconstructed surface, and similar strain values were observed for other systems.^{27,28} Adatom ejection from the constrained Au surface is thermodynamically hindered, with a calculated ΔG_{Def} value of 0.3 eV. However, the presence of MT adsorbates considerably reduced the vacancy-formation energy by ~ 0.6 eV, hence favoring adatom ejection. This result can be rationalized in

194 terms of a change of the metal–metal bond on the substrate
 195 because this gets weaker as the lattice constant decreases,²⁹
 196 hence making a contracted substrate considerably more reactive
 197 toward adatom expulsion. The presence of constrained regions
 198 of the surface with the adsorbed SAM should act as a temporary
 199 source of adatoms. However, once the strain is reduced, the
 200 adatom ejection will cease; therefore, other sources of Au
 201 adatoms should be considered.

202 The top bulk-terminated Au layer or atomic steps are the
 203 most natural sources and sinks of adatoms and vacancies.³⁰

204 Figure 1 displays calculated vacancy-formation Gibbs free

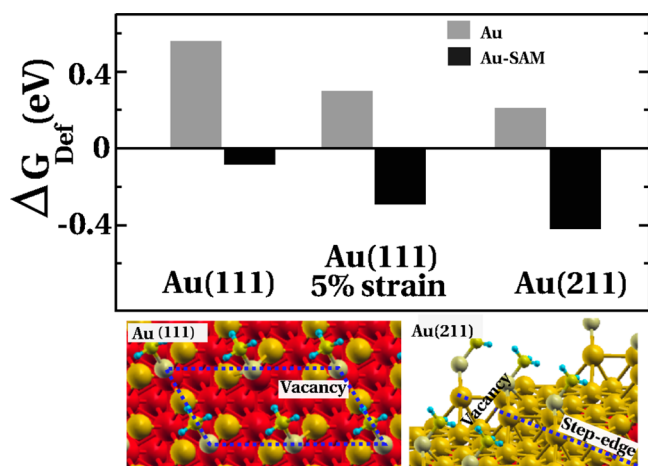


Figure 1. Vacancy-formation Gibbs free energies, ΔG_{Def} for a set of different Au motifs without (gray) or with (black) the presence of an adsorbed SAM: (left) Au (111), (center) Au(111) under uniaxial 5% compressive strain, and (right) Au (211) stepped surface. A schematic representation of the vacancy motifs is presented on the lower panel, where the bottom metal layers are colored red to highlight the surface vacancy.

205 energies for a set of different scenarios. The energy cost to
 206 remove a single Au atom from the (111) surface of gold is 0.58
 207 eV, in good agreement with previous estimates.³¹ The vacancy
 208 formation energy is considerably lower along the step edge. In
 209 fact, using Au(211) as a model for a stepped gold surface, our
 210 calculations predict ΔG_{Def} to be 0.17 eV at the step sites. The
 211 thermodynamic driving force is, however, not sufficient to make
 212 the adatom generation spontaneous, and very high temper-
 213 atures would be needed before a sizable fraction of surface Au–
 214 Au bonds are broken. Interestingly enough, our results indicate
 215 that the presence of the SAM largely reduces the vacancy
 216 formation energy. Our DF calculations predict the formation of
 217 gold vacancies within the SAM to be particularly favored at the
 218 step sites, with $\Delta G_{\text{Def}} = -0.4$ eV. The large detachment energy
 219 from the step edges suggests that SAM-decorated step edges
 220 may serve as an efficient source of Au atoms that tend to diffuse
 221 through the surface until fixed as adatoms. Adatom-stripping is
 222 also favored at the Au(111) terraces, where the influence of
 223 step edges should be less significant.

224 Because the concentration of surface vacancies correlates
 225 with the vacancy formation energy, our results indicate that the
 226 nucleation of the self-assembly will lead to a local increase in
 227 the equilibrium concentration of vacancies. The generation of
 228 surface defects follows the trend of higher reactivity for adatom
 229 stripping (and vacancy generation) at step edges and regions
 230 with localized strain within the self-assembly as compared with
 231 the higher-coordinated terrace sites. A defect concentration

gradient, established between the step edges and terraces, will
 232 produce a net mass flux of Au adatoms out (during assembly)
 233 or into the step edges (after assembly), causing the surface
 234 steps to shrink or enlarge. Indeed, adsorbate-promoted mass
 235 flow on Au(111) has been previously observed for other
 236 adsorbates.³² The excess defects released during monolayer
 237 assembly will incorporate into the self-assembly to equilibrate
 238 the surface.

Next, we apply ab initio atomistic thermodynamics to study
 240 the vacancy-pit nucleation in the presence of a self-assembly.
 241 The nucleation of pits is attributed to the condensation of
 242 vacancies, which are supersaturated as a consequence of the
 243 assembly process. Figure 2 (central left panel) displays Gibbs
 244 free energies of formation, ΔG_{SAM} for different coverage of
 245 vacancies arranged in the form of ordered islands of increasing
 246 size. On the one hand, the purely physical interaction between
 247 gas-phase DMDS molecules and pristine Au(111) (i.e., in the
 248 absence of Au vacancies) is enough to form spontaneously a
 249 SAM at RT (Figure 2, Structure 1). The inclusion of Au
 250 vacancies has profound consequences strongly affecting the
 251 stability of the SAM. Our results indicate that the incorporation
 252 of low concentrations of surface vacancies into the SAM is
 253 thermodynamically hindered and that under these conditions
 254 Au vacancies decrease the stability of the adsorbed phase.
 255 However, the nucleation of small vacancy-pits becomes
 256 spontaneous for Θ_{Def} larger than 0.18 ML. For large enough
 257 vacancy concentration, vacancy-pits will nucleate, reducing the
 258 local surface tension of the self-assembled phase. As shown in
 259 Figure 2 (top and bottom panels), MT moieties covering the
 260 vacancy pit preferentially bind to the low-coordinated site along
 261 the edge of the pit. The structure at $\Theta_{\text{Def}} = 0.18$ ML
 262 corresponds to an array of pit-like defects of $\sim 110 \text{ \AA}^2$ size
 263 with MT molecules decorating the bottom of the pit (Figure 2,
 264 Structure 5). This is in qualitative agreement with experimental
 265 observations, which found vacancy pits corresponding to
 266 vacancy coverage between 0.1 and 0.2 ML.¹ Particularly
 267 interesting is the fact that large enough pit-like structures are
 268 energetically competitive with defect-free phases, which suggest
 269 that the coalescence of small vacancy-pits might be possible.
 270 This suggests that for large enough vacancy pits the most
 271 relevant scenario at the interface corresponds to a transient
 272 situation where either pit-like structures or vacancy-free phases
 273 are stabilized. In fact, the coexistence of different phases was
 274 previously suggested by the authors.³³

Before further discussing the implications of the present
 276 findings, it is appropriate to assess to which extent calculated
 277 stability differences are to be trusted. To clarify this point
 278 further, we have carried a rigorous study of the systematic error
 279 in the calculated free energies. According to our previous
 280 ΔG_{SAM} definition, the Gibbs free energy difference per unit area
 281 between two phases with and without surface defects, with the
 282 same nature, under fixed external conditions is given by

$$\Delta\gamma = \frac{\Delta G_{\text{SAM}}(\Theta_{\text{Def}}) - \Delta G_{\text{SAM}}(\Theta_{\text{Def}=0})}{A} \approx \frac{\Delta E - E_{\text{Au}}^{\text{bulk}} \Delta N}{A} \quad (3)$$

where ΔN is the difference in the number of substrate atoms
 285 between the two models (i.e., number of defects on the
 286 reconstructed phase) and ΔE is the total energy difference
 287 between the two models. The absolute error in the free energy
 288 $\zeta_{\Delta\gamma}$ can be related to the error in total energy, ζ_E , as in eq 4

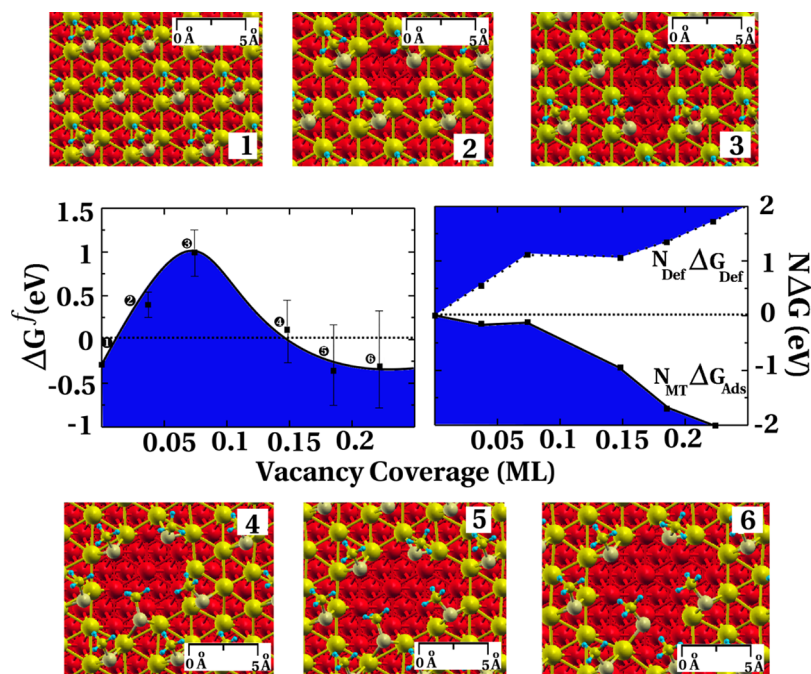


Figure 2. Central left panel: Gibbs free energy formation, ΔG_f^f , of a given SAM structure for different coverage of surface vacancies. Error bars are included to indicate the systematic error in the calculated Gibbs free energies. Central right panel: Contributions to the formation Gibbs free energy according to a simple splitting $\Delta G_{\text{SAM}} = N_{\text{Def}}\Delta G_{\text{Def}} + N_{\text{MT}}\Delta G_{\text{Ads}}$ for increasing surface vacancy concentrations. Lines are included as a guide to the eye. Top and bottom panels: plain view of the structures in the central panels. Au atoms on the first metal layer are highlighted in yellow, and bottom metal layers are colored red in order to highlight the distribution of surface vacancies on the structure.

$$\zeta_{\Delta\gamma}^2 = \left| \frac{\delta\Delta\gamma(E)}{\delta E} \right|^2 \zeta_E^2 = \Delta N^2 \zeta_E^2 \quad (4)$$

where one simply assumes that $\Delta\gamma$ is a function of E . To find a reasonable estimate of the error on the total energy, ζ_E , we suggest the use of the surface energy γ_{Clean} for the clean cell as $(1/2A)(E - E_{\text{Au}}^{\text{Bulk}}N_{\text{Au},0})$, where E and $N_{\text{Au},0}$ are the total energy of the unit cell and the number of Au atoms in it. The error in γ is given by

$$\zeta_{\gamma} \approx \pm \left| \frac{\partial\gamma_{\text{Clean}}(E)}{\partial E} \right| \zeta_E = \pm \left(\frac{1 - N_{\text{Au},0}}{2A} \right) \zeta_E \quad (5)$$

and hence $\zeta_{\Delta\gamma}$ can be expressed as

$$\zeta_{\Delta\gamma} = \pm \Delta N \left(\frac{2\zeta_{\gamma}A}{1 - N_{\text{Au},0}} \right) \quad (6)$$

which has two main contributions: one related to the difference in the number of atoms in the surface models considered and a second one related to the error in the total energy that needs to be estimated. Equation 6 deserves further comments because it controls the error in the Gibbs free energy calculations. It implies that one should avoid using the Gibbs free energy formalism as in ref 22 when ΔN is large or when the slab model is too small. The calculated value for γ_{Clean} in our work is 46 meV/Å², consistent with previous calculations,³⁴ whereas the experimentally derived value is 75 meV/Å².³⁵ The difference between both values is a well-known deficiency of the DF-GGA approach.³⁶ Taking into account the different values for ΔN for the different surface models considered in the letter, we have computed the error bars for the values in Figure 2, which are included in the central left panel.

We are now in a position to understand the reasons behind the impact of surface defects on the stability of SAMs. To do this, and following previous studies,³⁷ it is useful to make use of the formation Gibbs free energy of a self-assembled phase, ΔG_{SAM} , as the result of two contributions, $\Delta G_{\text{SAM}} = N_{\text{Def}}\Delta G_{\text{Def}} + N_{\text{MT}}\Delta G_{\text{Ads}}$. According to this simple splitting, the stability of a certain self-assembled structure relies on a subtle balance between two main contributions: (i) the lateral corrugation of the metallic substrate, included in ΔG_{Def} and (ii) the inter adsorbate forces and anchor bond strength, both included in the Gibbs free energy of adsorption, ΔG_{Ads} . The first contribution describes the energy required to form the defective Au substrate, whereas the Gibbs free energy of adsorption, $\Delta G_{\text{Ads}} = (1/N_{\text{MT}})(G_{\text{Tot}} - G_{\text{Cell}} - N_{\text{MT}}(\mu_{\text{DMDS}}/2))$ refers to the energy involved on MT bonding to the defective surface. These two opposing effects govern the stability of the SAM, and hence defect formation induced by the presence of the SAM will only occur if the binding energy increase is larger than the defect formation energy. Figure 2 (central right panel) gives both contributions to the formation Gibbs free energy. The Figure demonstrates that the formation of a defective substrate is thermodynamically unfavorable. More importantly, the Figure also demonstrates that defect-rich substrates generally bind MT stronger than defect-free Au surfaces. However, stronger binding of MT does not always imply larger stability, and for most of the defective structures studied in this work, the binding energy increase is smaller than the defect formation energy. Only at large enough vacancy coverage regime is the favorable binding of MT molecules sufficient to make the self-assembly a spontaneous process.

To summarize, the present results provide important insight into the role of surface defects on the molecular mechanism of SAM formation and reveal the active role that step edges play on the generation of gold adatoms and surface vacancies. The

349 local concentration of defects is increased due to self-assembly,
350 and vacancy pits will nucleate to equilibrate the surface. More
351 importantly, our calculations also show that atom-stripping and
352 vacancy-formation become thermodynamically favored even on
353 higher-coordinated terrace sites. This explains the formation of
354 vacancy pits on the terraces of Au, where the role of the step
355 edges is expected to be less significant. However, the
356 concentration of surface vacancies can also be limited by
357 other factors, and the diffusion of defects or the length of the
358 hydrocarbon chain will certainly play an important role in self-
359 assembly. Our results imply that forming virtually defect-free
360 monolayers would be a challenging task, and the amphiphile/
361 substrate interaction will naturally generate vacancy islands.

362 ■ AUTHOR INFORMATION

363 Present Address

364 ¹Center for Functional Nanomaterials, Brookhaven National
365 Laboratory, Upton, New York 11973, United States.

366 Notes

367 The authors declare no competing financial interest.

368 ■ ACKNOWLEDGMENTS

369 D.T. thanks Dr. Mark Hybertsen for fruitful discussions.
370 Calculations were performed on the *Marenostrum* super-
371 computer of the Barcelona Supercomputer Center. We are
372 grateful for the support by Spanish MICINN (grants FIS2008-
373 02238 and CTQ2011-24784), Generalitat de Catalunya (grants
374 2009SGR1041 and XRQTC), and Argentine ANPCyT (PICT
375 2010-2554). Finally, F.I. acknowledges additional support
376 through 2009 ICREA Academia award for excellence in
377 research.

378 ■ REFERENCES

- 379 (1) Vericat, C.; Vela, M. E.; Benitez, G.; Carro, P.; Salvarezza, R. C.
380 *Chem. Soc. Rev.* **2010**, *39*, 1805.
381 (2) Maksymovych, P.; Voznyy, O.; Dougherty, D. B.; Sorescu, D. C.;
382 Yates, J. T., Jr. *Prog. Surf. Sci.* **2010**, *85*, 206.
383 (3) Love, J. C.; Estroff, L. A.; Kriebel, J. K.; Nuzzo, R. G.; Whitesides,
384 G. *Chem. Rev.* **2005**, *105*, 1103.
385 (4) Vericat, C.; Vela, M. E.; Salvarezza, R. C. *Phys. Chem. Chem. Phys.*
386 **2005**, *7*, 3258.
387 (5) Maksymovych, P.; Sorescu, D. C.; Yates, J. T., Jr. *J. Phys. Chem. B*
388 **2006**, *110*, 21161.
389 (6) Mazzarello, R.; Cossaro, A.; Verdini, A.; Rousseau, R.; Casalis, L.;
390 Danisman, M. F.; Floreano, L.; Scandolo, S.; Morgante, A.; Scoles, G.
391 *Phys. Rev. Lett.* **2007**, *98*, 016102.
392 (7) Maksymovych, P.; Sorescu, D. S.; Yates, J. T., Jr. *Phys. Rev. Lett.*
393 **2006**, *97*, 146103.
394 (8) Yu, M.; Bovet, N.; Satterley, C. J.; Bengió, S.; Lovelock, K. R. J.;
395 Milligan, P. K.; Jones, R. G.; Woodruff, D. P.; Dhanak, V. *Phys. Rev.*
396 *Lett.* **2006**, *97*, 166102.
397 (9) Pensa, E.; Cortes, E.; Corthey, G.; Carro, P.; Vericat, C.;
398 Fonticelli, M. H.; Benitez, G.; Rubert, A. A.; Salvarezza, R. C. *Acc.*
399 *Chem. Res.* DOI: 10.1021/ar200260p.
400 (10) Somorjai, G. A. *Surf. Sci.* **1979**, *89*, 496.
401 (11) Behrens, M.; Studt, F.; Kasatkin, I.; Kühn, S.; Hävecker, M.;
402 Abild-Pedersen, F.; Zander, S.; Girsig, F.; Kurr, P.; Knief, B. L.;
403 Tovar, M.; Fischer, R. W.; Nørskov, J. K.; Schlögl, R. *Science* **2012**,
404 *336*, 893.
405 (12) Vang, R. T.; Honkala, K.; Dahl, S.; Vestergaard, E. K.; Schnadt,
406 J.; Lægsgaard, E.; Clausen, B. S.; Nørskov, J. K.; Besenbacher, F. *Nat.*
407 *Mater.* **2005**, *4*, 160.
408 (13) Liu, Y.; Ozolins, V. J. *Phys. Chem. C* **2012**, *116*, 4738.
409 (14) Poirier, G. *Langmuir* **1997**, *13*, 2019.
410 (15) Poirier, G. E.; Pylant, E. D. *Science* **1996**, *272*, 1145.

- (16) Blöchl, P. *Phys. Rev. B.* **1994**, *50*, 17953. 411
(17) Perdew, J.; Wang, Y. *Phys. Rev. B* **1992**, *45*, 13244. 412
(18) Molina, L. M.; Hammer, B. *Chem. Phys. Lett.* **2002**, *360*, 264. 413
(19) Kondoh, H.; Iwasaki, M.; Shimada, T.; Amemiya, K.; Yokoyama,
T.; Ohta, T.; Shimomura, M.; Kono, S. *Phys. Rev. Lett.* **2003**, *90*, 414
066102. 415
(20) Touzov, I.; Gorman, C. B. *J. Phys. Chem. B* **1997**, *101*, 5263. 416
(21) Monkhorst, H. J.; Pack, J. D. *Phys. Rev. B* **1976**, *13*, 5188. 417
(22) Kresse, G.; Furthmüller, J. *Comput. Mater. Sci.* **1996**, *6*, 15. 418
(23) Reuter, K.; Scheffler, M. *Phys. Rev. B* **2001**, *65*, 035406. 419
(24) Carling, K.; Wahnstrom, G.; Mattsson, T. R.; Mattsson, A. E.;
Sandberg, N.; Grimvall, G. *Phys. Rev. Lett.* **2000**, *85*, 3862. 420
(25) Mukherjee, K. *Philos. Mag.* **1965**, *12*, 915. 421
(26) Benny, S.; Grau-Crespo, R.; De Leeuw, N. H. *Phys. Chem. Chem.*
Phys. **2009**, *11*, 808. 422
(27) Barth, J. V.; Brune, H.; Ertl, G.; Behm, R. J. *Phys. Rev. B* **1990**,
42, 9307. 423
(28) Wintterlin, J.; Zambelli, T.; Trost, J.; Greeley, J.; Mavrikakis, M. 424
Angew. Chem., Int. Ed. **2003**, *42*, 2850. 425
(29) Mavrikakis, M.; Hammer, B.; Nørskov, J. K. *Phys. Rev. Lett.* 426
1998, *81*, 2819. 427
(30) Burton, W. K.; Cabrera, N.; Frank, F. C. *Philos. Trans. Roy. Soc.* 428
London **1951**, *243*, 299. 429
(31) Eremeev, S. V.; Lipnitskii, A. G.; Potekaev, A. I.; Chulkov, E. V. 430
Russ. Phys. J. **1997**, *40*, 276. 431
(32) Peale, D. R.; Cooper, B. H. *J. Vac. Sci. Technol. A* **1992**, *10*, 2210. 432
(33) Torres, D.; Carro, P.; Salvarezza, R. C.; Illas, F. *Phys. Rev. Lett.* 433
2006, *97*, 226103. 434
(34) Migani, A.; Illas, F. *J. Phys. Chem. B* **2006**, *110*, 11894. 435
(35) Brophy, J. H.; Rose, R. M.; Wulff, J. *Thermodynamics of* 436
Structure; Wiley: New York, 1964; p 1870. 437
(36) Vitos, L.; Ruban, A. V.; Skriver, H. L.; Kollár, J. *Surf. Sci.* **1998**, 438
411, 186. 439
(37) Molina, L. M.; Hammer, B. *Chem. Phys. Lett.* **2002**, *360*, 264. 440
441
442
443
444